Construction and Building Materials 114 (2016) 87–97

Contents lists available at ScienceDirect

Construction and Building Materials

journal homepage: www.elsevier.com/locate/conbuildmat

Concrete cover characterisation using dynamic acousto-elastic testing and Rayleigh waves

Quang Anh Vu [a,*], Vincent Garnier [a], Jean François Chaix [a], Cédric Payan [a], Martin Lott [a], Jesus N. Eiras [b]

[a] Aix-Marseille Université, LMA UPR 7051, IUT Aix-en-Provence, 413 Av. Gaston Berger, 13100 Aix-en-Provence, France
[b] Instituto de Ciencia y Tecnología del Hormigón (ICITECH), Universitat Politècnica de València, Camino de Vera s/n, 46022 València, Spain

HIGHLIGHTS

- Dynamic acousto-elastic testing by using Rayleigh waves as probe wave and the first bending mode excitation as pump wave.
- Nonlinear dynamic acousto-elastic behaviour of concrete.
- High relative variation of nonlinear parameters for assessment of thermally damage concrete and carbonated concrete.
- The method opens up new possibilities for in situ measurement.

ARTICLE INFO

Article history:
Received 1 October 2015
Received in revised form 9 March 2016
Accepted 20 March 2016
Available online 31 March 2016

Keywords:
Nondestructive evaluation
Concrete cover
Surface Rayleigh wave
Dynamic acousto-elastic testing
Conditioning
Thermal damage
Carbonation

ABSTRACT

This paper presents the application of surface Rayleigh waves in nonlinear dynamic acousto-elastic testing for the nondestructive evaluation of the concrete cover. Numerous physical phenomena, such as conditioning and slow dynamics, characterising the dynamic non-classical nonlinear elastic behaviour of many types of micro-heterogeneous solids, were observed in concrete. Rayleigh waves were used as probing waves to evaluate the effect of local property changes in a concrete cover. The proposed method was validated for two typical problems of concrete durability, in a case of thermal damage – distributed micro-damage – and in a case of carbonation – surface problem with determination of the carbonation depth. In both cases, the results showed that the relative variation as a function of material changes of the nonlinear parameters was much higher than that of the ultrasonic pulse velocity.

1. Introduction

This research falls within the civil engineering context of nondestructive evaluation (NDE) by ultrasound of concrete [1], and particularly of concrete cover. The external 3–5 cm concrete structure layer is most affected by various environmental factors. This layer acts as a passive film that protects the reinforcing bars from environmental impacts. Most concrete structures are large and it is difficult to conduct measurements on these structures using transmitted waves. The use of Rayleigh waves requiring only one-sided access to a structure shows potential for monitoring the integrity of concrete cover. Rayleigh waves are mechanical waves that propagate along the free surface of a solid, and transfer most of their energy to the near-surface region [2]. The effective depth of penetration of a Rayleigh surface wave is approximately one wavelength. The Rayleigh wave velocity is approximately 90–92% of the shear wave velocity. In literature, variations in Rayleigh wave velocity and attenuation have been widely studied in NDE for cement-based material characterisation [3–5]. Recently, classical nonlinear measurements based on the second harmonic generation of Rayleigh waves have been developed to evaluate near-surface nonlinearities for different concrete structures [6,7]. These recent developments allow for evaluations of either linear acoustic parameters or classical nonlinear parameters.

Concrete is a strongly heterogeneous material. The elastic behaviour of concrete-like materials is known as being nonlinear strain-dependent [8–12]. In the nonlinear elastic theory of Murnaghan [8], where a strain above 10^{-4} is applied to a material by quasi-static solicitation, acousto-elastic measurements showed that the elastic modulus variation is a linear function of the strain amplitude. This linear variation allows for the experimental extraction of the third order elastic constants l, m and n [13–15]. At lower strain amplitude, 10^{-7}–10^{-5}, under dynamic solicitation, the mate-

* Corresponding author.
E-mail address: quanganhdhgt@gmail.com (Q.A. Vu).

http://dx.doi.org/10.1016/j.conbuildmat.2016.03.116
0950-0618/

rial exhibits hysteresis during loading cycles. This behaviour has been studied in some types of rock [19–23]. Once the material is stressed dynamically, its elastic properties decrease and it reaches a nonequilibrium dynamic state [9]. The material now is considered as being conditioned. Thus, the nonlinear evolution of the modulus is described as a function that includes high order strain terms, strain amplitude and strain rate [10].

$$M(\varepsilon,\dot{\varepsilon}) = M_0\{1+\beta\varepsilon+\delta\varepsilon^2+\ldots+\alpha[\Delta\varepsilon,\varepsilon\cdot sign(\dot{\varepsilon})]\} \quad (1)$$

In Eq. (1), M_0 is the linear elastic modulus; $\Delta\varepsilon$ is the local strain amplitude variation, $\dot{\varepsilon} = d\varepsilon/dt$ is the strain rate, $sign(\varepsilon) = 1$ if $\dot{\varepsilon} > 0$ and $sign(\varepsilon) = -1$ if $\dot{\varepsilon} < 0$. The parameters β and δ are the classical quadratic and cubic nonlinear parameters of the classical nonlinear theory, respectively, whereas α is a nonclassical nonlinear parameter that represents material hysteresis. Note that Eq. (1) is a phenomenological description of fast dynamics, especially for NDE applications. It does not include slow dynamics that correspond to the time-dependent recovery of the elastic properties after a disturbance. In this study, the slow dynamics were also observed experimentally, but were not analysed.

Many NDE nonlinear acoustic techniques, such as nonlinear wave modulation spectroscopy (NWMS) [24] and nonlinear resonant ultrasound spectroscopy (NRUS) [25], are based on the model in Eq. (1). According to the general trend observe from these studies, nonlinear acoustic parameters showed a much higher sensitivity to material changes than linear measurement parameters, particularly to damage-associated changes. In the literature on cement-based materials (mortar and concrete), nonlinear acoustic techniques showed their efficiency in evaluating different ageing problems due to mechanical or environmental impacts, for example corrosion of the reinforcing bars [26], alkali-silica reaction [27,28], static mechanical loading [29,30], thermal damage [31–34], carbonation [7,35,36].

Among nonlinear techniques, dynamic acousto-elastic testing (DAET) is noticed as providing a more complete insight into the acoustic nonlinearity exhibited by micro-inhomogeneous media like granular and cracked materials. This recently developed method [16–22] allows us to analyse the elastic behaviour of the material during entire loading cycles. Thus, both the classical and nonclassical parameters can be extracted. Based on the "pump-probe" principle [15], we chose to use a Rayleigh wave as probe wave in our measurement for its ability to conduct local inspection. A technique based on a similar principle to study indirect and semi-indirect transmission configurations was presented by Bui et al. [37]. In this reference study, only one high frequency pulse was used as probe wave, whereas the pump wave was generated by a mechanical impact. The nonlinearity information extracted was the sum of time shifts analysed by using a window sliding over the probe signal.

Our proposed methodology was applied to thermal damage and carbonation of concrete. Thermal damage is in the form of distributed micro-cracking and it was showed that the nonlinear parameters were highly sensitive to the evolution of this damage [31–34]. Carbonation depth evaluation represents a gradual surface problem, which is still a challenge for nondestructive techniques.

In this paper we analyse the nonlinear parameters measured in a DAET experiment using Rayleigh waves, applying the technique to two typical concrete durability problems. In the first section the mechanisms of thermal damage and carbonation are described, and information on the concrete samples is given. Next, all the DAET experimental conditions are explained. The results are discussed and then compared with results reported in the literature. Finally, we provide conclusions on nonlinear Rayleigh wave ultrasonic measurement, and propose some prospects.

2. Materials and methods

2.1. Materials

In this part, the description of microstructural changes occurring in concrete caused by thermal damage and carbonation is presented. Each case study consisted of a series of concrete samples. Before being tested for nonlinear DAET measurement, all the samples were characterised based from velocity measurements. The elastic modulus and Poisson's ratio were thus estimated according to their reciprocal relationship with the pressure velocity and shear wave velocity. The density of each sample was quantified by the ratio between mass and volume. All these values are presented in detail in the next section.

Bulk wave measurement was performed by transmission, while Rayleigh wave measurement was performed using two contact piezoelectric transducers mounted on two wedges to generate an incident wave with a specific angle. The measurements of both the pressure wave velocity and Rayleigh wave velocity were made using two Panametrics-NDT ultrasonic transducers (model V101, central frequency 250 kHz). Two Panametrics-NDT transducers (model V151, central frequency 250 kHz) were used for shear wave velocity measurements.

As for the generation of the Rayleigh waves, the wedges were made of Polytetrafluoroethylene (PTFE), in which the pressure wave velocity is 1250 m/s. The wedge inclination angle had been set at 45° – which is generally bigger than the second critical angle of all the samples – to attenuate the bulk waves as much as possible during Rayleigh wave generation. It was observed that the bandwidth of a Rayleigh wave in a concrete sample was limited at about 170 kHz. Beyond this limit, the signal-to-noise ratio of the received signal was very low. Thus, we chose to work with 100 kHz waves for different reasons. The source signal was set as an impulse-type signal – one cycle burst at 100 kHz with 150 V of input voltage. The frequency spectrum of the received signal is centred at 90 kHz. The first reason for the choice of frequency and high voltage was to achieve a good signal-to-noise ratio for the Rayleigh waves. The second reason was that Rayleigh waves were considered as propagating within approximately 22 mm of the surface layer (corresponding to one wavelength). Therefore, the carbonation depth in all the carbonated concrete samples presented below could be covered by the penetration depth of the Rayleigh wave.

2.1.1. Thermal damage

Thermal damage is referred to for concrete structures (e.g., domestic residences, tunnels) in the context of fire attacks or for radioactive waste packages that continue to radiate heat. At 105 °C, free water and physically adsorbed water evaporate [17]. The porous structure of concrete is slightly modified. Upon heating to 400 °C, the total porosity increases gradually. The network of interconnected pores resulting from micro-cracking becomes coarser. At 450–500 °C, chemical reactions begin, which leads to changes in the microstructure. Above these temperatures, concrete becomes severely damaged.

In this work, experimental tests were conducted on four prismatic concrete samples ($90 \times 90 \times 260$ mm^3). The concrete had a water cement ratio of 0.44 and contained fine aggregates of maximum size $d_{max} = 8$ mm. Samples were cured for more than 28 days and were subjected to different heat treatments – T1 was kept intact and T2, T3 and T4 were heated to 180 °C, 250 °C and 400 °C – involving 24 h heating in a furnace and 24 h cooling. Sample designations and measured properties are summarised in Table 1.

The main consequence of a heat treatment (heating and cooling) is the generation of distributed cracks and a decrease in density as a function of temperature. An increase in volumetric degradation due to heat treatment is indicated by the decrease in bulk wave and Rayleigh wave velocities.

2.1.2. Carbonation

What is called carbonation is the progressive formation of calcium carbonate in concrete due to the penetration of carbon dioxide (CO_2) from air (there is a small amount of CO_2 in the pores) that reacts with calcium hydroxide $Ca(OH)_2$ in the cement paste. The chemical reactions can be described as [35]:

$$CO_2 + H_2O \rightarrow H_2CO_3$$

Table 1
Thermally damaged samples data.

Designation	T1	T2	T3	T4
Heat treatment	Intact	180 °C	250 °C	400 °C
ρ (kg/m^3)	2240	2131	2128	2119
$V_{pressure}$ (m/s)	4628	3927	3718	3008
V_{shear} (m/s)	2578	2307	2236	1838
$V_{Rayleigh}$ (m/s)	2354	2106	2042	1678
E (GPa)	38.5	28.0	25.9	17.2
ν	0.275	0.236	0.217	0.202

$$H_2CO_3 + H_2O \rightarrow HCO_3^- + H_3O^+$$

$$HCO_3^- + H_2O \rightarrow CO_3^{2-} + H_3O^+$$

The reaction between carbonic acid and carbon dioxide in the cement paste after dissolution is:

$$H_2CO_3 + Ca(OH)_2 \rightarrow CaCO_3 + 2H_2O \quad (2)$$

The direct consequence of these reactions is a decrease in the pH of the affected zone. Consequently, reinforcing steel loses its passive film protection and the risk of corrosion increases significantly. As carbon dioxide penetrates into the concrete from outside, the outer layer is the most exposed.

The carbonation series consisted of three $120 \times 250 \times 500$ mm^3 concrete samples, with three different thicknesses of the carbonated layer: 5 mm, 10 mm and 20 mm. The accelerated carbonation, in which carbon dioxide could attack only one face of the sample, was carried out in the lab. The affected depth in each sample was verified on duplicate samples that had undergone identical treatment. Sample designations and some measured properties are listed in Table 2. Only Rayleigh wave velocities increased regularly as a function of the carbonation depth whereas bulk wave velocities did not change. This result can be explained by the ratio between propagation zone and carbonation depth. Indeed, Rayleigh waves propagated within a layer of approximately 22 mm under the surface, which is of the same order as the carbonated concrete depth, whereas bulk waves penetrated into the sample to a depth of 120 mm and provided volumetric information.

2.2. A nonlinear acoustic method: dynamic acousto-elastic testing (DAET)

DAET measurements are based on the "pump-probe" principle. A first low frequency (LF) high amplitude wave, called "pump wave" disturbs the material and highlights its nonlinear behaviour. Concrete is thus conditioned and exhibits nonequilibrium dynamics. A second high frequency (HF) wave, called "probe wave", is a series of low-amplitude pulses. Pulses are sent at different times to measure the elastic changes generated by LF for different levels of strain. It is assumed that the probe wave does not disturb the material. The method computes the nonlinear propagation time shifts of the HF pulses. These time shifts are denoted time of flight modulations (TOFM). They characterise material nonlinearities due to the LF solicitation. The variation in elastic modulus induced by the LF perturbation as measured by DAET is deduced from Eq. (3) [19]:

$$\frac{\Delta M}{M_0} = \frac{M_\varepsilon - M_0}{M_0} \approx -\frac{2}{TOF_0} TOFM \quad (3)$$

where TOF_0 is the time of flight of an HF pulse without LF perturbation. Based on Eq. (1), Renaud et al. [19] proposed a practical approach where the relative variation in elastic modulus as a function of strain during loading cycles under steady state can be fitted by a second-order polynomial (Eq. (4)).

$$\frac{\Delta M}{M_0} \approx \delta\varepsilon^2 + \beta\varepsilon + C \quad (4)$$

In this approach, δ and β represent classic nonlinear effects and C measures the conditioning offset which depicts a non-classical nonlinear manifestation. In literature, longitudinal waves have been used as "probe waves" for DAET in some kinds of stone [18–22]. The use of surface Rayleigh wave in DAET measurement for evaluating nonlinear properties of concrete cover is presented and discussed for the first time in this paper.

2.2.1. Experimental setup

The experimental setup is represented in Fig. 1. The shaker generated LF vibrations that disturbed the concrete sample with the first bending mode (pump wave), while the Rayleigh wave (probe wave) pulses were generated simultaneously to auscultate the surface layer. The wave generation system consisted of two wave generators (Tektronix AFG 3102 and generation card ARB), and two oscilloscopes for signal acquisition (Lecroy 24MXs-A, Lecroy HDO 4024). The trigger systems of the generators and oscilloscopes were interconnected so that all the signals were synchronised. Two oscilloscopes were used to record the signals, to acquire more

Table 2
Carbonated samples data.

Designation	C1	C2	C3
Carbonation depth (mm)	5	10	20
ρ (kg/m^3)	2267	2277	2283
$V_{pressure}$ (m/s)	4191	4001	4173
V_{shear} (m/s)	2393	2356	2423
$V_{Rayleigh}$ (m/s)	1987	2064	2153
E (GPa)	32.7	31.2	33.4
ν	0.258	0.235	0.246

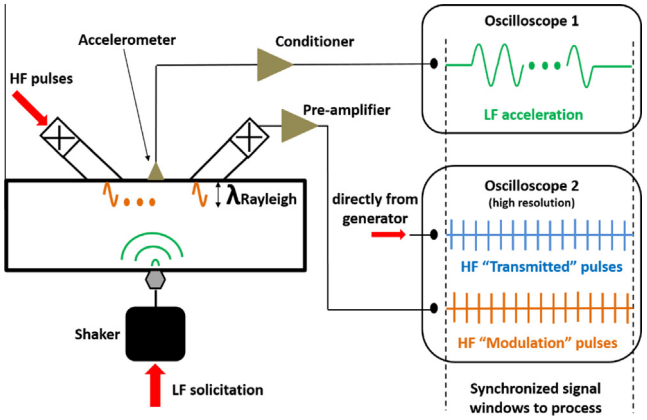

Fig. 1. DAET setup; green signal: LF acceleration, blue signal: "Transmitted" pulses, orange signal: "Modulation" pulses. (For interpretation of the references to colour in this figure legend, the reader is referred to the web version of this article.)

points and a higher resolution. This fact is particularly important for HF signals in view of the very fine time shift (up to 10^{-9} s) that would be analysed from these signals.

For LF generation, the range of resonant frequencies for each sample was ascertained by an eigen-frequency analysis using simulation software (Comsol Multiphysics®), and their effective values were found experimentally. The resonant frequencies found experimentally corresponding to the first bending mode at the lowest excitation level were 3988 Hz, 3322 Hz, 3100 Hz and 2636 Hz for samples T1, T2, T3 and T4, respectively, while they were 1536 Hz, 1530 Hz and 1488 Hz for samples C1, C2 and C3, respectively. Therefore, an evolution of resonance frequencies as a function of thermal damage was observed in thermally damaged samples, whereas the same evolution was not observed in carbonated samples. This result showed a good coherence with velocities measurement (Table 2). For a single test at any excitation level, a sinusoidal burst containing about five hundred cycles of LF was generated to reach the steady state and maintain it. Vibration was measured as an acceleration by an accelerometer that was glued to the centre of the measuring surface (Fig. 1). Synchronised with the LF burst signal, two series of HF 100 kHz pulses were sent. In fact, LF vibration was turned on only after 50 ms from the first HF pulse. This allowed several pulses to propagate into the sample without being disturbed by the LF field, and, thus, the reference time of flight (TOF_0) to be calculated. The first pulse signal was a low voltage signal sent directly to the oscilloscope. The recorded signal, marked in blue in Fig. 1, was termed "transmitted" signal. The second pulse signal was a high voltage signal (150 V). It generated Rayleigh waves into the concrete sample. The recorded Rayleigh wave pulse signal was termed "modulation" signal, and is marked in orange in Fig. 1. The availability of the transmitted signal helped on the one hand to calculate the time of flight of each modulation pulse (before LF and with LF), and on the other hand to avoid effects of temporal drift in the generation system on the calculated time of flight. Positioning the HF transducers in the central zone of the sample allowed probe wave inspection in the most stressed zone in the first bending solicitation mode.

All DAET conditions were taken into account in this configuration. Firstly, the "quasi-static" condition requires that the propagation time of an HF pulse in the material (TOF_0) should be at least one tenth of the LF period [18]. In this study, the first bending mode was chosen for the LF excitation. The LF frequency of each sample is presented above. The distance between the transducers (see Fig. 2a) was set for different practical reasons. The placed distances of 2 cm and 8 cm were chosen for the thermally damaged samples and the carbonated samples, respectively. These distances led to a ratio of just below one tenth between the propagation time of the HF pulse in the concrete and the LF period. This regulation helped to assume that the strain during the time of flight of each HF pulse is constant. Secondly, the "quasi-uniform" condition requires that the strain field established over the HF beam width should be spatially constant [18]. Indeed, in this study we considered the nonlinear effect to be only due to the deformation component upon wave direction. By considering the investigated Rayleigh wave pulse penetration depth relative to the sample thickness, we assumed that the considered deformation component within this depth would be constant. The determination of deformation for the first bending mode will be presented in more details in the next section.

Pulses were regularly spaced in time, which corresponded to a repetition frequency (f_{rep}). The temporal distance between two consecutive pulses is presented as Eq. (5).

$$f_{rep} = \frac{1}{T_{rep}} = \frac{1}{t_{pulse(i+1)} - t_{pulse(i)}} \quad (5a)$$

$$\text{with } t_{pulse(i+1)} = t_{pulse(i)} + n \cdot T_{LF} + \frac{1}{16} T_{LF} \quad (5b)$$

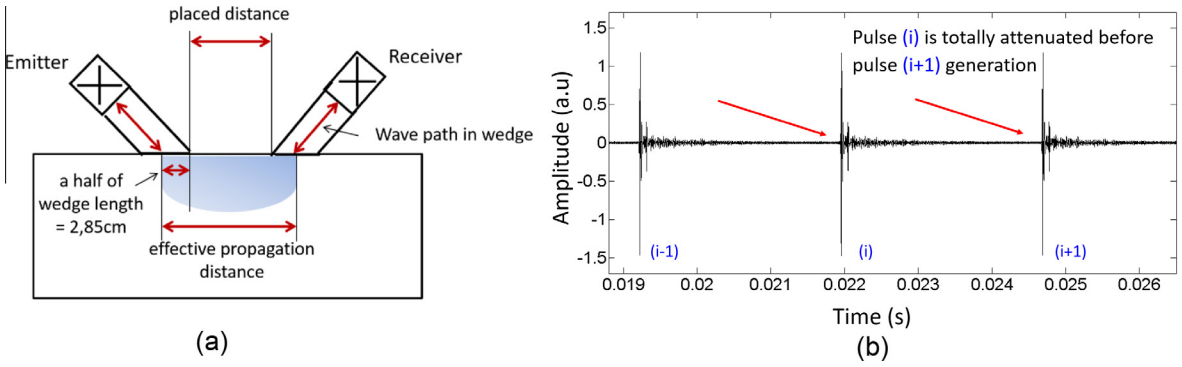

Fig. 2. Experimental conditions; (a) conventions of wave paths, (b) illustration of two consecutive modulation pulses.

where T_{LF} (s) is the LF period and n is an integer that denotes the number of LF periods that was chosen to ensure the absence of signal overlap (Fig. 2b). With this procedure, there were about two hundred pulses in total and about one hundred pulses positioned within steady regime. In fact, the f_{rep} in the tests was obtained by rounding the f_{rep} obtained according to Eq. (5a). Consequently, the corresponding positions of these pulses in the LF signal were placed automatically with a shift between them. There were thus more than sixteen different strain values over the loading cycle. In order to obtain a wider distribution of HF pulses corresponding to different strain values, the test for one excitation level was repeated two times with a relative delay of $T_{ref}/2$ between LF and HF signals. As a result, more than thirty-two different strain amplitude values were analysed for each excitation level. Each acquisition was an average of ten sending times, with 30 s between two consecutive sendings. Furthermore, from the analysis that showed that nonlinearity is a function of LF perturbation amplitude, each sample was tested for four LF excitation levels corresponding to four input voltages of the shaker. The highest excitation level corresponded to the maximum voltage that could be used to excite the shaker without saturation of the accelerometer signal recorded. A big shaker (B&K type 4809) was used for the carbonation tests because of the large sample dimensions.

2.2.2. Analysis of DAET

Nonlinear time shifts are normally quantified by comparison between modulation signals and transmitted signals. To this end, a windowing process was applied for the transmitted and modulation signals. Fig. 3 shows the illustration of a unique temporal window applied over the two signals, as they are synchronised.

The window length was chosen so that only coherent Rayleigh wave portions were selected (Fig. 3). Thus, only the Rayleigh wave contributions were included in the time shift analysis. The synchronisation of the transmitted and modulation signals allowed us to eliminate generator drift thanks to the windowing process.

The total time of flight of a modulation pulse can be understood as the sum of its time of flight in concrete and twice its time of flight in the wedges. This full path propagation time could be quantified as the time shift between the current modulation pulse and the corresponding transmitted pulse using cross-correlation. A second-order fit was applied afterwards over three points around the maximum value of cross-correlation, in order to search for the oversampling peak. This allowed the time shift to be estimated as being of the order of 10^{-9} s [18]. Then, for each modulation pulse we considered only the time of flight into concrete $TOF_C(i)$. This time corresponds to the wave path in concrete, which was conventionalised and determined by the distance between two wedge centres. Twice the time of flight in one wedge (T_{wedge}) was then subtracted, according to Eq. (6):

$$TOF_C(i) = TOF(i) - 2 \cdot T_{wedge} \tag{6}$$

The TOFM of each pulse was obtained from Eq. (7)

$$TOFM(i) = TOF_C(i) - TOF_{C\text{-}0} \tag{7}$$

in which $TOF_{C\text{-}0}$ designates TOF_0 in Eq. (3), corresponding to the mean reference time of flight into concrete for j pulses recorded before LF activation.

To analyse the displacements and the deformations of the sample, we based ourselves on the relation between the experimentally measured out-of-plane acceleration and these components obtained from a numerical simulation in Comsol®. This algorithm was proposed and applied by Payan et al. [33,38]. The numerical model used real sample dimensions and elastic properties (presented in Tables 1 and 2) computed from wave velocities in each state (Fig. 4a). Such exploitation allowed us to correct the linear time shift due to geometric changes that can be understood as wave path changes in the propagation direction because of flexural vibration. The displacement in the propagation direction dl_{yy} was estimated from the measured out-of-plane acceleration and their ratio by a numerical model.

$$dl_{yy} = \frac{dl_{yy\_model}}{a_{z\_model}} \cdot a_{z\_measured} \tag{8}$$

in which dl_{yy_model} and a_{z_model} are respectively the displacement and acceleration extracted from the eigen-frequency analysis of the first bending mode simulation, $a_{z\_measured}$ is the acceleration measured experimentally by the accelerometer. The time shift due to the linear geometric effect was computed afterwards as the ratio between the estimated displacement and the Rayleigh wave velocity. The final experiment $TOFM_{exp}$ is described by Eq. (9), after correcting geometric changes considered as representing only nonlinear effects.

$$TOFM_{exp}(i) = TOFM(i) - \frac{dl_{yy}}{V_{Rayleigh}} \tag{9}$$

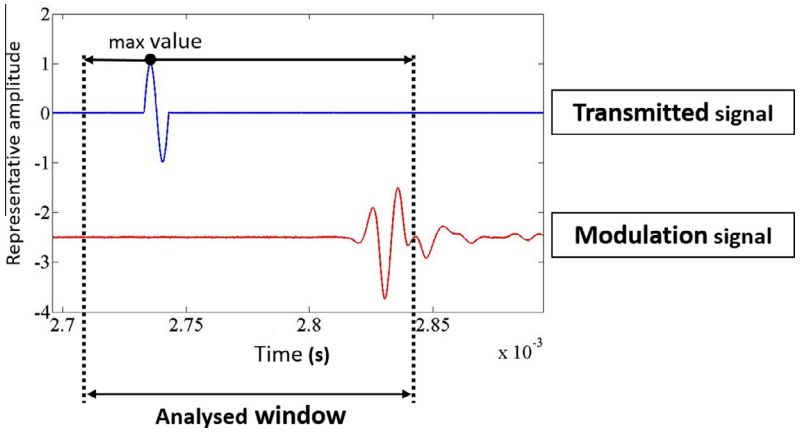

Fig. 3. Description of the windowing process over the transmitted signal and the modulation signal.

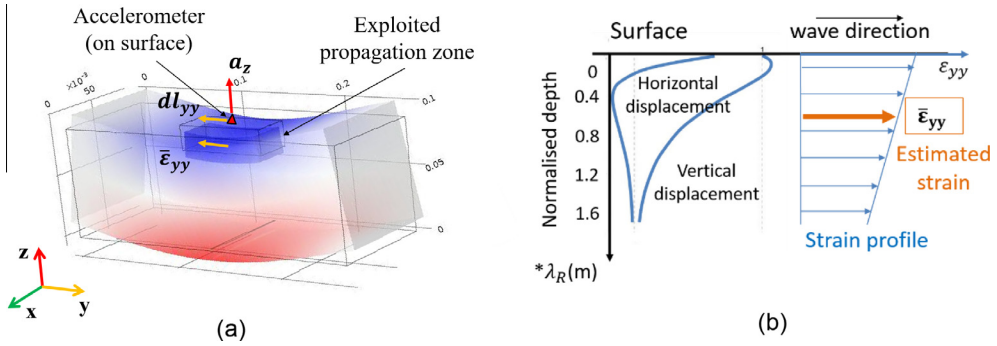

Fig. 4. Estimation of displacement and strain thanks to the measured acceleration and their ratio from linear simulation model in Comsol®.

For illustration, in the case of an excitation level maximum for sample T1, the estimated displacement (dl_{yy}) was about 10^{-7} m. Thus, the linear time shift caused by the geometric changes was about 3×10^{-10} s – about 1% of the nonlinear time shift caused by the modulation effect ($TOFM_{exp}$). The same order for the corrected time was found for the other samples. This geometric effect can be very important either in the case of materials and pathologies presenting small differences between the nonlinear time shift ($TOFM_{exp}$) and the linear time shift ($dl_{yy}/V_{Rayleigh}$), or in the case of a great distance between transducers. We conclude that such effect should be taken into account for all measurements in which the first bending mode is exploited.$TOFM_{exp}$ in Eq. (9) corresponds to TOFM in Eq. (3), and was applied to obtain nonlinear parameters according to the approach in Eq. (4). The determination of strain in Eq. (4) is based on the principle presented above for estimating displacement. Indeed, we considered, in the first bending mode of the current configuration (in plane yOz), the strain components that concern two polarisations of the Rayleigh wave pulse (upon Oy and Oz). According to the values quantified from the simulation results, the vertical strain component ε_{zz} is equal to 0.23 times the horizontal strain component ε_{yy}. We assumed in this study that the nonlinear time shift effect of Rayleigh wave propagation was due principally to the strain component which is parallel to the wave propagation direction (ε_{yy}) [15]. Furthermore, most of the Rayleigh wave energy is located within a one-wavelength layer under the surface. In this study, we proposed an approach for strain determination, in which the effective strain $\bar{\varepsilon}_{yy}$ is the mean value of strain over the propagation volume. The proposed propagation volume can be described as a rectangular parallelepiped – its length measured the distance between the wedge centres, its width measured the wedge width and its height measured one wavelength of Rayleigh wave (Fig. 4a). This effective strain was estimated thanks to the measured acceleration according to Eq. (10), and was used afterwards as the strain value in Eq. (4) for nonlinear parameter extraction.

$$\bar{\varepsilon}_{yy} = \frac{\bar{\varepsilon}_{yy\_model}}{a_{z\_model}} \cdot a_{z\_measured} \tag{10}$$

Fig. 5a shows an example of the relative variation in elastic modulus ($\Delta M/M_0$) as a function of acquisition time. A decrease in elastic modulus due to LF excitation and an offset of its variation corresponding to a nonequilibrium metastable state can be observed. Fig. 5b presents the signature of nonlinear elasticity ($\Delta M/M_0$ as a function of $\bar{\varepsilon}_{yy}$) in which the black curve recalls the second order polynomial approach of Eq. (4). A positive axial LF strain corresponds to a tensile axial strain, whereas a negative axial LF strain corresponds to a compressive axial strain. Positioning the pulse at the same strain value over LF cycles may induce the same variation in modulus. Over one cycle, a hysteretic behaviour is recognised from the dissymmetry between increasing and decreasing strain. According to Eq. (4), δ, β and C represent the curvature, the slope and the offset, respectively, of the parabola that fits the set of points (black curve in Fig. 5b). Physically, the conditioning offset C can represent the nonequilibrium metastable state of the material induced by the LF excitation.

3. Results and discussion

Concrete exhibits a nonlinear response with increasing disturbance amplitude. To characterise the state of the material, NDE analyses the evolution of nonlinear parameters as a function of strain amplitude. The strain amplitude ($\Delta\varepsilon$) corresponding to each excitation level was defined as the maximum strain value (Fig. 5b), which was estimated from Eq. (10). We present in the following section the evolution of three nonlinear parameters (δ, β and C) as a function of strain amplitude. According to these evolutions, some qualitative nonlinear parameters will be proposed and their relative variations will be compared with velocity measurements.

3.1. Thermal damage

The maximum value of strain amplitude that could be reached without signal saturation in the case of sample T1 was 6.15×10^{-6}, 6.58×10^{-6} for sample T2, 7.54×10^{-6} for sample T3 and 4.08×10^{-6} for sample T4. For illustration, Fig. 6a and b show all nonlinear elasticity curves for the intact sample T1 and the thermally damaged sample T3, while Fig. 6c presents each one of the samples chosen such that their corresponding strain amplitudes are of the same order. All the vertical axes in Fig. 6 have the same scale. The curves for the damaged samples were observed as being generally more open than those for the undamaged samples. Note that no term in the second order polynomial-based approach in Eq.

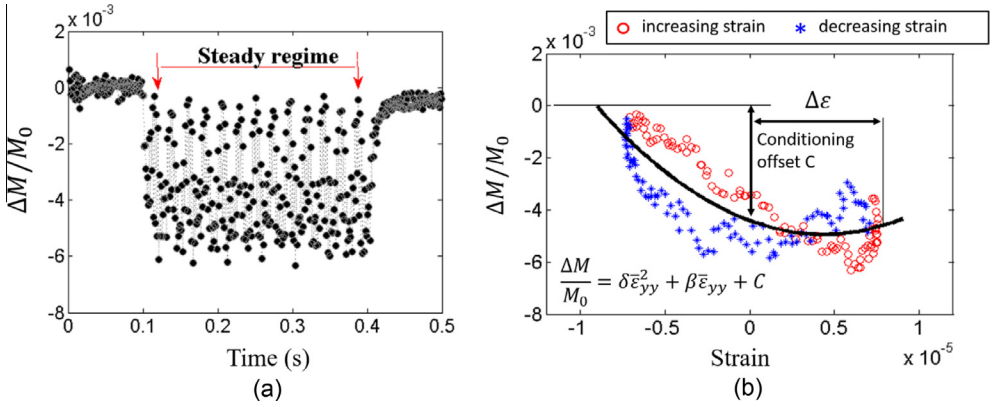

Fig. 5. Illustration of resulting curves from signal analysis in the case of sample T1 at the fourth excitation level, (a) $\Delta M/M_0$ of all pulses as a function of acquisition time; (b) $\Delta M/M_0$ of the pulses positioned in steady regime as a function of $\bar{\varepsilon}_{yy}$.

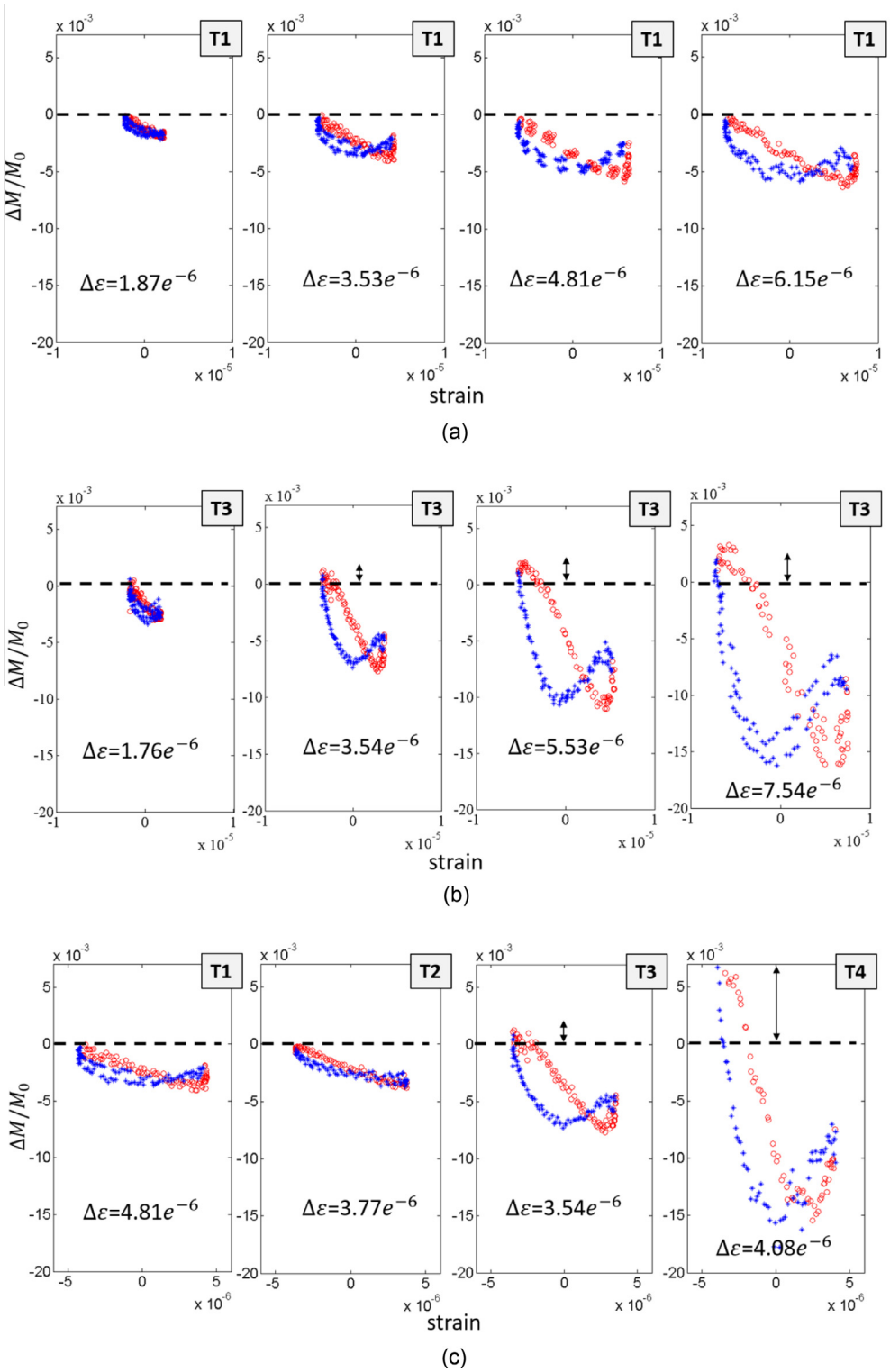

Fig. 6. Relative variation of elastic modulus ($\Delta M/M_0$) as a function of ε corresponding to (a) four excitation levels in the case of sample T1, (b) four excitation levels in the case of sample T3, (c) approximately same strain amplitudes between all thermally damaged samples. The red circles represent an increasing strain while the blue asterisks represent a decreasing strain. (For interpretation of the references to colour in this figure legend, the reader is referred to the web version of this article.)

(4) represents mathematically the opening. We assumed that the opening is one of the nonlinear acoustic signatures of the concrete hysteretic behaviour during a loading cycle.

The evolution of nonlinear parameters (δ, β and C) is presented in Fig. 7a, b and c as a function of strain amplitude. Parameters β and C were negative whereas δ was positive. There was no obvious trend in the evolution of δ and β as a function of strain amplitude. We thus proposed in this study an approach that considers the mean values of δ and β, designated by $\bar{\delta}$ and $\bar{\beta}$ – determined as in Eqs. (11) and (12).

$$\bar{\delta} = \frac{\sum_{i=1}^{k} \delta(\Delta\varepsilon_i)}{k} \tag{11}$$

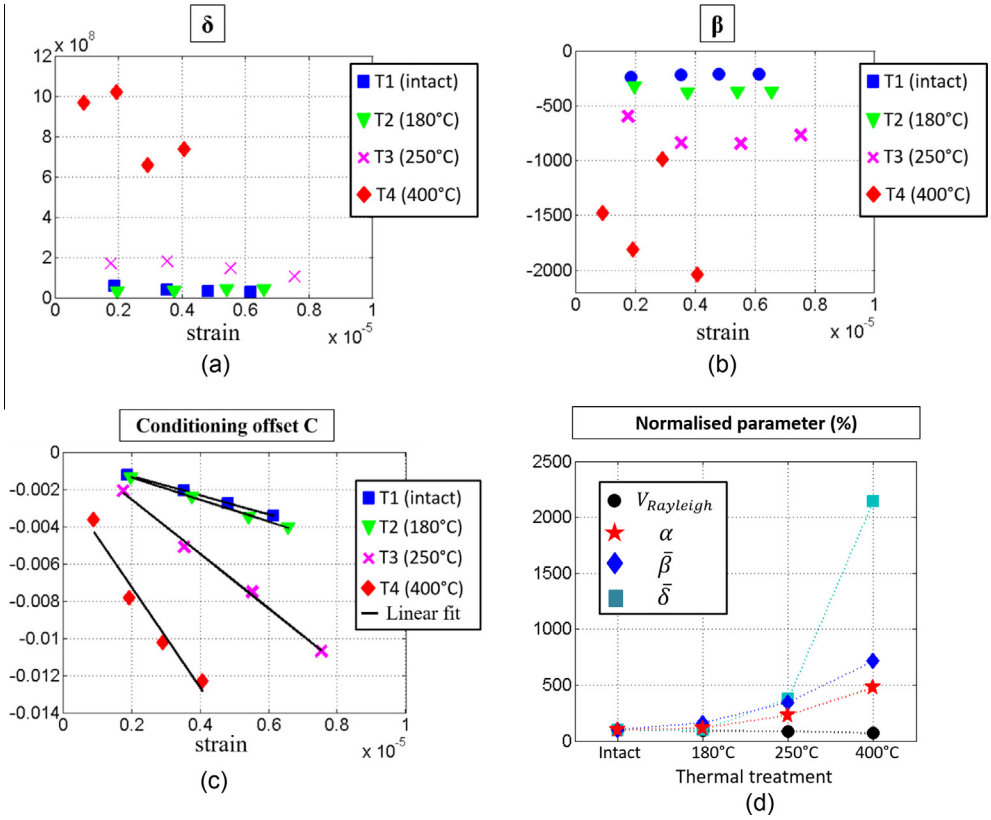

Fig. 7. DAET results for the thermal damage, (a) evolution of δ as a function of strain amplitude, (b) evolution of β as a function of strain amplitude, (c) evolution of C as a function of strain amplitude, (d) comparison of relative variation between linear and nonlinear parameters as a function of thermal damage.

$$\bar{\beta} = -\frac{\sum_{i=1}^{k}\beta(\Delta\varepsilon_i)}{k} \tag{12}$$

In this study $k = 4$, corresponding to four LF excitation levels. Therefore, these parameters, $\bar{\delta}$ and $\bar{\beta}$, represented the level of thermal damage (their values are given in Table 3).

As for the conditioning offset C, its absolute value increased significantly in function of strain amplitude (Fig. 7c) and follows a linear variation. Thus, parameter α representing hysteretic behaviour was introduced to determine the slope of the evolution of C (Eq. (13)), and represented the level of thermal damage (Table 3).

$$\alpha = -\frac{C}{\Delta\varepsilon} \tag{13}$$

The relative variation of the nonlinear parameters in the DAET analysis was compared afterwards with that of the Rayleigh wave velocity (which is a linear acoustic parameter). Considering that sample T1 (intact sample) was the normalisation reference, the values of its normalised parameters were set at 100%. The parameters of the other samples were then normalised with respect to the corresponding parameters of sample T1, and were given values in percent (%). The result in Fig. 7d shows the much higher relative variation as a function of thermal damage of the nonlinear parameters than of the Rayleigh wave velocity. In extreme cases, between the most damaged sample T4 and the sound sample T1, $\bar{\delta}$ differed by as much as twenty times, seven times for $\bar{\beta}$ and nearly five times for α, while the Rayleigh wave velocity decreased 0.3 times (30%).

Table 3
Nonlinear parameters of thermal damage analysis.

Samples	T1 (intact)	T2 (180 °C)	T3 (250 °C)	T4 (400 °C)
$\bar{\beta}$	2.2×10^2	3.6×10^2	7.6×10^2	15.8×10^2
$\bar{\delta}$	3.9×10^7	3.8×10^7	14.9×10^8	84.5×10^7
α	5.1×10^2	5.8×10^2	11.7×10^2	24.1×10^2

3.2. Carbonation

The nonlinear parameters for concrete carbonation were analysed in the same manner as were those for thermal damage. In this study, only one Rayleigh wave frequency was used to evaluate different carbonation depths. As presented above, by generating 100 kHz Rayleigh wave pulses, the carbonation depth in all the carbonated concrete samples (the maximum case carbonation depth is 20 mm of sample C3) could be covered by the penetration depth of the Rayleigh wave (approximatively 22 mm of the surface layer). By this fact, we assumed that the effect of carbonated concrete on the Rayleigh wave propagation could be obtained. The maximum value of strain amplitude that could be attained without signal saturation in the case of sample C1 was 3.68×10^{-6}, 3.37×10^{-6} for sample C2 and 3.66×10^{-6} for sample C3. In general, the curves that characterised a nonlinear elastic modulus variation in carbonation samples (Fig. 8) were more closed than those that characterised the same variation in thermally damaged samples.

The evolution of δ, β and C as a function of strain amplitude is presented in Fig. 9. Indeed, δ carries a different (negative) sign for sample C2, whereas β is almost constant, and so the mean value approach can thus be considered acceptable. The conditioning offset C obeys linear evolution as a function of strain amplitude. By applying a mean value approach to δ and β, and a linear approach to C, the result indicates that these proposed parameters evolved inversely as a function of the carbonation depth. Indeed, the value of $\bar{\beta}$ for sample C3 was 30% that of sample C1. The difference between these two samples in terms of value of α was 50%, while

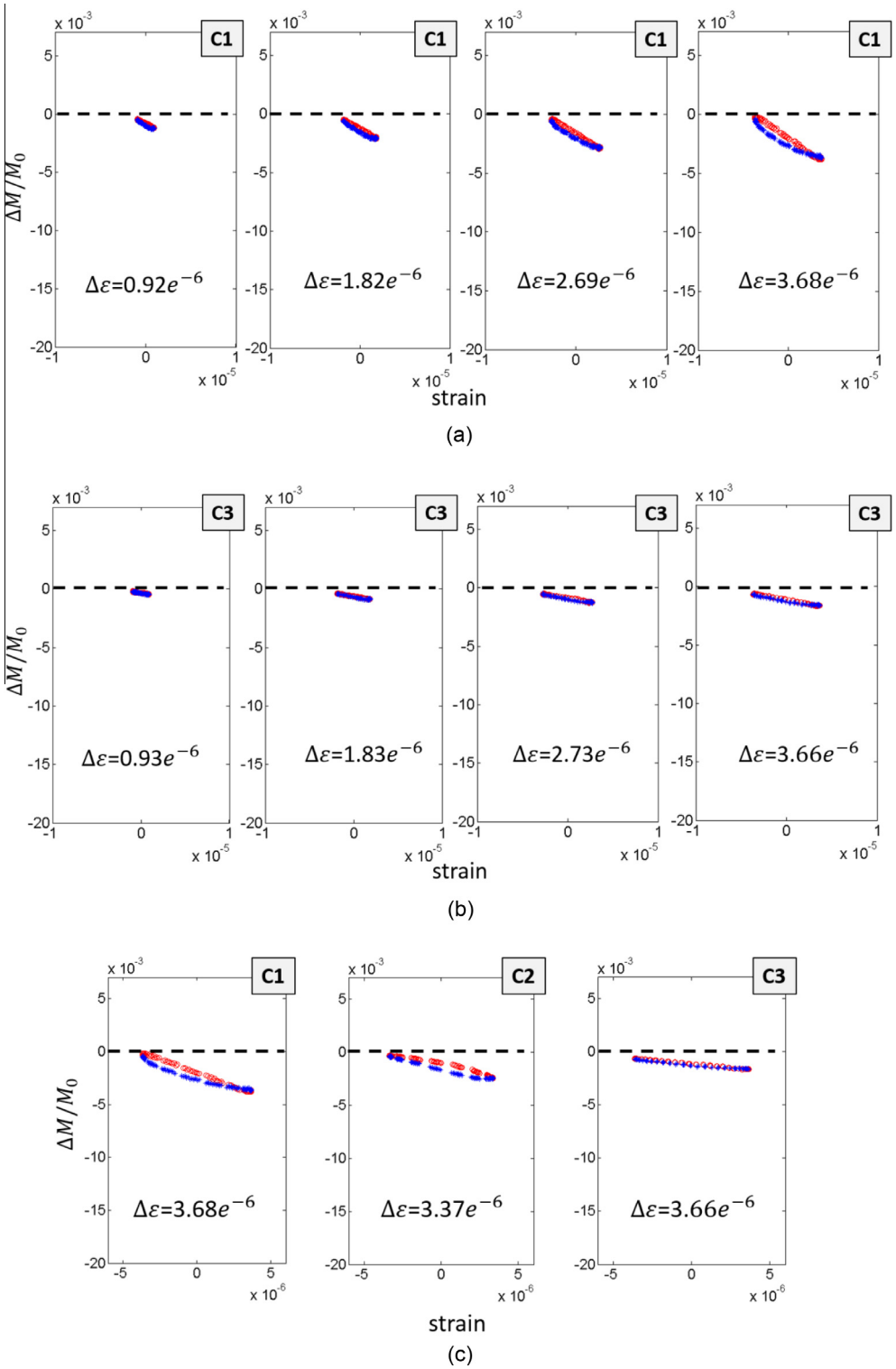

Fig. 8. Relative variation of elastic modulus $\Delta M/M_0$ as a function of ε corresponding to (a) four excitation levels in the case of sample C1, (b) four excitation levels in the case of sample C3, (c) approximately the same strain amplitudes for all the carbonated samples. The red circles represent an increasing strain while the blue asterisks represent a decreasing strain. (For interpretation of the references to colour in this figure legend, the reader is referred to the web version of this article.)

that from velocity measurements was only 8%. This result means that the sample that presents a higher carbonation depth has smaller nonlinear parameter values. All nonlinear parameter values for the carbonation analysis are given in Table 4.

3.3. Discussion

This part consists of discussions about the result of this work, how it can be linked to the microstructure of concrete, as well as to improvements of the measurement technique.

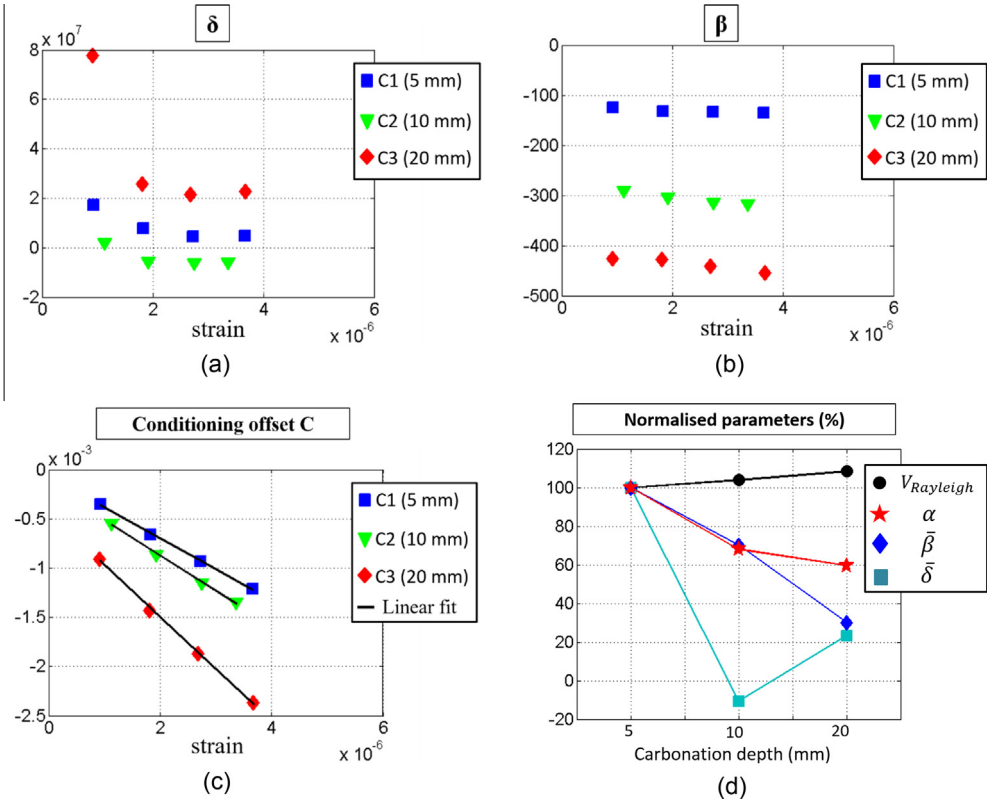

Fig. 9. DAET results for the carbonation analysis, (a) evolution of δ as a function of strain amplitude, (b) evolution of β as a function of strain amplitude, (c) evolution of C as a function of strain amplitude, (d) comparison of the relative variations of the linear and nonlinear parameters as a function of carbonation.

Table 4
Nonlinear parameters for the carbonation analysis.

Sample carbonation depth (mm)	C1	C2	C3
	5	10	20
$\bar{\beta}$	4.4×10^2	3.1×10^2	1.3×10^2
$\bar{\delta}$	3.7×10^7	-0.4×10^7	0.9×10^7
α	5.3×10^2	3.6×10^2	3.1×10^2

The first discussions concern the conformity of the results with the literature. The absolute values of δ, β and C were determined as being of the same order as the equivalent parameters presented in the literature. Indeed, the classical nonlinear parameters, δ and β, were of the same order as those obtained by Renaud et al. [19] for Berea stone. In that reference study, δ and β were almost constant within the strain amplitude interval from 10^{-7} to 5×10^{-6}. Thus, the mean value approach can be considered acceptable.

As for the nonclassical parameter C, in general, a good linear fit was observed for its dependence on strain amplitude. The absolute values of α in the case of thermal damage (from 5×10^2 to 25×10^2) are comparable with those determined by Payan et al. [33] in the quantitative study of thermal damage in ordinary concrete using the NRUS method. In addition, the same evolution trend of carbonation nonlinear parameters was obtained by means of another technique, such as NRUS by Bouchaala et al. [35], nonlinear Rayleigh wave harmonic generation based method by Kim et al. [7], and nonlinear impact resonant acoustic spectroscopy (NIRAS) by Eiras et al. [36]. Parameter α as a perspective could be an effective parameter for concrete nonlinearity evaluation. Furthermore, by referring to the power law exponents proposed by Scalerandi et al. [39], the linear dependence observed in this study between conditioning offset and strain amplitude (Eq. (13)) in both cases, thermally damaged concrete and carbonated concrete, led to the same value of the exponent b = 1. As a results, thermally damaged concrete and carbonated concrete were considered as being classed in the class B. According to these authors [39], the class B contains in general consolidated granular and cellular media exhibiting nonlinear hysteretic behaviour. Thus, the linear dependence approach proposed in this study showed a good agreement with the power law analysis proposed by the authors. This result confirms our expectation that nonlinearities originate from a density of nonlinear contacts [9,39]. In systems exhibiting brick-mortar features (i.e., hard-soft and fragile portions) in general, and particularly in concrete, a nonlinear contact can be localized at the interface between soft and hard portions of materials, i.e., in the region between grains or between cracks.

The second discussion is about the repeatability and reproducibility of the measurements. These kinds of measurement are not presented in this paper. We propose here to consider the problem by referring to the literature studies on the same methods. Indeed, the repeatability and reproducibility of velocity measurements are generally good. The coefficient of variation was found 1.62% for pressure wave velocity in transmission configuration and 2% for the Rayleigh wave velocity [1]. In the case of big changes in the elastic properties of the material (like, for instance in sample T4), velocity measurements can be a reliable technique. However, nonlinear behaviour allows getting insight on the type of nonlinearity. So nonlinear parameters complement linear parameters. In addition, in the context of early damage characterisation, the nonlinear techniques should be more interesting due to the high sensitivity of the nonlinear parameters. Renaud et al. [18] studied the precision of the DAET technique for the nonlinear parameters of Lavoux Limestone by repeating the measurement three times in the same conditions. In this reference work [18], while δ seemed to be highly varied, the slope β and the offset C have a coefficient of variation between 3% and 8%. These authors also indicated two

possible causes of the scattering in TOFM. The first cause relates to the performance of the waveform generator used to excite the US probe in terms of phase and amplitude jitters. In this respect, we used the transmitted signal, which was synchronised with the modulation signal. This synchronisation helped to avoid any electronic effect for the calculation of the time modulation. The second cause of scatter in TOFM was determined by the signal to noise ratio of the received probe wave signals. The authors ([18]) took this ratio into account since they used a head wave, which is usually a weak signal in terms of amplitude. Conversely, the Rayleigh wave (presented in Fig. 4) was detected as the first arrival and showed a very good signal to noise ratio. In short, even some experimental conditions could be discussed by considering influential factors analysed in the literature, it is noted that to obtain a reliable measurement method all experiment conditions should be taken into account. A part of our future work will concern the testing of the repeatability and reproducibility of the current method.

The last discussion highlights the links between concrete nonlinearity and its microstructure in two cases, thermally damaged concrete and carbonated concrete, through the evolution of the nonlinear parameters. Firstly, it was observed that the absolute values of α for thermally damaged concrete are bigger than those for carbonated concrete. Note that thermally damaged concrete was assumed to contain distributed micro-cracks, whereas carbonated concrete has a lower porosity that leads to a higher elastic modulus than that of non-carbonated concrete. Therefore, these results showed good correlation between the evolution of parameter α and the evolution of nonlinearities in concrete, provided these nonlinearities originate from a density of nonlinear contacts (micro-cracks, porosities, etc.) [9].

Secondly, some interesting points can be discussed when observing the nonlinear elasticity signatures (curves representing $\Delta M/M_0$ as a function of ε). Indeed, it was observed that for approximately identical strain amplitudes, the curves for greatly thermally damaged concrete samples are more open than those for sound concrete and carbonated concrete samples (Figs. 6c and 8c). In addition, the maximum value of $\Delta M/M_0$ can be subject of discussion. This value of $\Delta M/M_0$ in fact corresponds to the maximum strain value in compression attained in each test. It seems that for not severely damaged concrete (as in the case of samples T1 and T2) or carbonated concrete (as in the case of samples C1, C2 and C3), the maximum value of $\Delta M/M_0$ in compression is smaller than or equal to zero. Conversely, this value for thermally damaged concrete (samples T3 and T4) could be greater than zero. A positive value of $\Delta M/M_0$ means that the elastic modulus of a material under compression is higher than that of a material in its initial state without mechanical solicitation. In order to account for these observations, it is suggested that the cracks opening in concrete in its initial state would close under compression solicitation, which would result in a denser material and consequently in higher wave velocities. On the contrary, the modulus of a material with no opening cracks or containing a small number of micro-cracks, even in compression state, may not exceed the modulus of the initial state Therefore, DAET measurement can contribute to the discrimination between thermal damage and carbonation in concrete.

To sum up, the proposed experimental method showed a remarkable evolution of nonlinear parameters as a function of thermal damage and carbonation depth. Absolute value of nonlinear parameters was found to be of the same order as those obtained in the literature. It is acknowledged that this study needs to be tested for the repeatability and for other samples. These tests will be a part of our future work.

To complement this study, it is suggested that the obtained results need to be explained by a good understanding – numerically and analytically – of the nonlinear behaviour of concrete. Recently, Lombard et al. [40] proposed a numerical model where the nonlinear hysteretic behaviour can be explained through taking the viscoelasticity of the material into account. A simulation model based on this approach and taking into account not only the mechanisms of thermal damage and carbonation but also the interaction between Rayleigh waves and the heterogeneous microstructure of concrete could open up explanatory prospects.

4. Conclusion

This research associates nonlinear acoustic DAET and surface Rayleigh waves to assess two typical concrete problems – thermal damage and carbonation. DAET can be used to analyse the strain dependence of the modulus and reveal the hysteretic behaviour of concrete, whereas Rayleigh waves are an advantageous tool for in-situ measurements. The use of the transmitted signal provides a good and reliable technique for time delay processing, particularly for correlating automatically the coherent wave parts and avoiding any electronic effects. Classical nonlinear parameters δ and β as well as nonclassical nonlinear conditioning offset C were analysed. The proposed nonlinear parameters $\bar{\delta}$, $\bar{\beta}$ and α showed higher relative variations as a function of elastic properties changes than the wave velocity. If the results for thermal damage help to validate the proposed method, then the carbonation results open up possibilities for nonlinear acoustic applications using surface Rayleigh waves to evaluate gradual problems. The proposed measurement method will soon be tested for repeatability and reproducibility. For the final objective of in-situ measurements in which a simple and efficient evaluation is usually required, a natural dynamic perturbation, such as the passage of a truck or a train on a bridge, could be used to generate the deformation. Otherwise, one-sided measurement using hammer impact and Rayleigh wave could be a first solution to following the evolution of material changes on site. These research prospects will be considered within the project DCND (Dynamic and Nondestructive Testings).

Acknowledgements

The authors acknowledge support from the French Agency of Research (ANR) through the project EVADEOS (EVAluation non destructive pour la prédiction de la DEgradation des structures et l'Optimisation de leur Suivi), the project ENDE (Evaluation Non Destructives des Enceintes de confinement des centrales nucléaires) and the project DCND (Dynamique et Contrôls Non Destructifs). The Laboratoire Matériaux et Durabilité des Constructions (LMDC) in Toulouse, France is also thanked for the production and carbonation treatment of the samples.

References

[1] V. Garnier, B. Piwakowski, O. Abraham, G. Villain, C. Payan, J.F. Chaix, Acoustic techniques for concrete evaluation: improvements, comparisons and consistency, Constr. Build. Mater. 43 (2013) 598–613.
[2] J. Popovics, O. Abraham, Surface wave techniques for the evaluation of concrete structures, in: Non-Destructive Evaluation of Reinforced Concrete Structures, vol. 2, WOODHEAD PUBLISHING, 2010, pp. 441–465.
[3] O. Abraham, B. Piwakowski, G. Villain, O. Durand, Non-contact auto-mated surface wave measurements for the mechanical characterisation of concrete, Constr. Build. Mater. 37 (2012) 904–915.
[4] L.J. Jacobs, J.O. Owino, Effect of aggregate size on attenuation of rayleigh waves in cement-based materials, J. Eng. Mech. 126 (11) (2000) 1124–1130.
[5] Dimitrios G. Aggelis, Tomoki Shiotani, Experimental study of surface wave propagation in strongly heterogeneous media, in: J. Acoust. Soc. Am. 122 (5) (2007) EL151–EL157.
[6] G. Kim, C.-W. In, J.-Y. Kim, K.E. Kurtis, L.J. Jacobs, Air-coupled detection of nonlinear Rayleigh surface waves in concrete-application to microcracking detection, NDT and E Int. 67 (2014) 64–70.

[7] G. Kim, J.Y. Kim, K.E. Kurtis, L.J. Jacobs, Y. Le Pape, M. Guimaraes, Quantitative evaluation of carbonation in concrete using nonlinear ultrasound, Mater. Struct. 49 (1) (2016) 399–409.
[8] F.D. Murnaghan, Finite deformations of an elastic solid, Am. J. Math. 59 (2) (1937) 235–260.
[9] R.A. Guyer, P.A. Johnson, Nonlinear mesoscopic elasticity: evidence for a new class of materials, Phys. Today 52 (4) (1999) 30–36.
[10] Van Den Abeele, Filip Koen et Windels, Characterization and imaging of microdamage using nonlinear resonance ultrasound spectroscopy (NRUS): an analytical model, in: Universality of Nonclassical Nonlinearity, Springer, New York, 2006, pp. 369–388.
[11] M. Bentahar, H. El Aqra, R. El Guerjouma, M. Griffa, M. Scalerandi, Hysteretic elasticity in damaged concrete: quantitative analysis of slow and fast dynamics, Phys. Rev. B 73 (1) (2006) 014116.
[12] A.S. Gliozzi, Marco Scalerandi, Modeling dynamic acousto-elastic testing experiments: validation and perspectives, J. Acoust. Soc. Am. 136 (4) (2014) 1530–1541.
[13] D.M. Egle, D.E. Bray, Measurement of acousto-elastic and third order elastic constants for rail steel, J. Acoust. Soc. Am. 60 (3) (1976) 741–744.
[14] C. Payan, V. Garnier, J. Moysan, P.A. Johnson, Determination of third order elastic constants in a complex solid applying code wave interferometry, Appl. Phys. Lett. 94 (1) (2009) 011904.
[15] I. Lillamand, J.-F. Chaix, M.-A. Ploix, V. Garnier, Acoustoelastic effect in concrete material under uni-axial compressive loading, NDT and E Int. 43 (8) (2010) 655–660.
[16] N. Ichida, T. Sato, M. Linzer, Imaging the nonlinear ultrasonic parameter of a medium, Ultrason. Imaging 5 (4) (1983) 295–299.
[17] Guillaume Renaud et al., Exploration of trabecular bone nonlinear elasticity using time-of-flight modulation, IEEE Trans. Ultrason. Ferroelectr. Freq. Control 55 (7) (2008) 1497–1507.
[18] Guillaume Renaud, Samuel Callé, Marielle Defontaine, Remote dynamic acoustoelastic testing: elastic and dissipative acoustic nonlinearities measured under hydrostatic tension and compression, Appl. Phys. Lett. 94 (1) (2009) 011905.
[19] G. Renaud et al., Nonlinear elastodynamics in micro-inhomogeneous solids observed by head-wave based dynamic acoustoelastic testing, J. Acoust. Soc. Am. 130 (6) (2011) 3583–3589.
[20] G. Renaud, P.-Y. Le Bas, P.A. Johnson, Revealing highly complex elastic nonlinear (anelastic) behaviour of earth materials applying a new probe: dynamic acoustoelastic testing, J. Geophys. Res. 117 (B6) (2012).
[21] G. Renaud et al., Hysteretic nonlinear elasticity of Berea sandstone at low-vibrational strain revealed by dynamic acousto-elastic testing, Geophys. Res. Lett. 40 (4) (2013) 715–719.
[22] G. Renaud et al., Anisotropy of dynamic acoustoelasticity in limestone, influence of conditioning, and comparison with nonlinear resonance spectroscopy, J. Acoust. Soc. Am. 133 (6) (2013) 3706–3718.
[23] J. Rivière et al., Pump and probe waves in dynamic acousto-elasticity: comprehensive description and comparison with nonlinear elastic theories, J. Appl. Phys. 114 (5) (2013) 054905.
[24] K.E.A. Van Den Abeele, P.A. Johnson, A. Sutin, Nonlinear elastic wave spectroscopy (news) techniques to discern material damage, part I: nonlinear wave modulation spectroscopy (nwms), Res. Non-Destr. Eval. 12 (1) (2000) 17–30.
[25] K.E.A. Van Den Abeele, J. Carmeliet, J.A. Ten Cate, P.A. Johnson, Nonlinear elastic wave spectroscopy (NEWS) techniques to discern material damage, part II: single-mode nonlinear resonance acoustic spectroscopy, Res. Non-Destr. Eval. 12 (1) (2000) 31–43.
[26] Paola Antonaci, Caterina Letizia Elisabetta Bruno, Marco Scalerandi, et al., Effects of corrosion on linear and nonlinear elastic properties of reinforced concrete, Cem. Concr. Res. 51 (2013) 96–103.
[27] K.J. Lesnicki, J.-Y. Kim, K.E. Kurtis, L.J. Jacobs, Characterization of ASR damage in concrete using nonlinear impact resonance acoustic spectroscopy technique, NDT and E Int. 44 (2011) 721–727.
[28] F. Moradi-Marani, A.S. Kodjo, P. Rivard, C.-P. Lamarge, Nonlinear acoustic technique of time shift for evaluation of alkali-silica reaction damage in concrete structures, ACI Mater. J. 111 (2014) 1–12.
[29] Van Den Abeele, De Visscher, Damage assessment in reinforced concrete using spectral and temporal nonlinear vibration techniques, Cem. Concr. Res. 30 (9) (2000) 1453–1464.
[30] P. Antonaci, C.L.E. Bruno, A.S. Gliozzi, M. Scalerandi, Monitoring evolution of compressive damage in concrete with linear and nonlinear ultrasonic methods, Cem. Concr. Res. 40 (7) (2010) 1106–1113.
[31] C. Payan, V. Garnier, J. Moysan, P.A. Johnson, Applying nonlinear resonant ultrasound spectroscopy to improving thermal damage assessment in concrete, J. Acoust. Soc. Am. 121 (4) (2007) 125–130.
[32] H.J. Kim, J.H. Kim, S.-J. Park, H.-G. Kwak, Characterization of thermally damaged concrete using a nonlinear ultrasonic method, Cem. Concr. Res. 42 (2012) 1438–1446.
[33] Cedric. Payan et al., Quantitative linear and nonlinear resonance inspection techniques and analysis for material characterization: application to concrete thermal damage, J. Acoust. Soc. Am. 136 (2) (2014) 537–546.
[34] J.N. Eiras et al., Non-classical nonlinear feature extraction from standard resonance vibration data for damage detection, J. Acoust. Soc. Am. 135 (2014) EL82–EL87.
[35] F. Bouchaala, C. Payan, V. Garnier, J. Balayssac, Carbonation assessment in concrete by nonlinear ultrasound, Cem. Concr. Res. 41 (5) (2011) 557–559.
[36] J.N. Eiras, T. Kundu, J.S. Popovics, J. Monzo', M.V. Borrachero, J. Paya', Effect of carbonation on the linear and nonlinear dynamic properties of cement-based materials, Opt. Eng. 55 (1) (2016) 011004.
[37] D. Bui et al., Evaluation of concrete distributed cracks by ultrasonic travel time shift under an external mechanical perturbation: study of indirect and semi-direct transmission configurations, J. Nondestr. Eval. 32 (1) (2013) 25–36.
[38] Cedric Payan et al., Probing material nonlinearity at various depths by time reversal mirrors, Appl. Phys. Lett. 104 (14) (2014) 144102.
[39] Marco Scalerandi et al., Evidence of microstructure evolution in solid elastic media based on a power law analysis, Commun. Nonlinear Sci. Numer. Simul. 22 (1) (2015) 334–347.
[40] Nicolas Favrie, Bruno Lombard, Cédric Payan, Fast and slow dynamics in a nonlinear elastic bar excited by longitudinal vibrations, Wave Motion 56 (2015) 221–238.